

Estimates of the reproduction ratio from epidemic surveillance may be biased in spatially structured populations

Piero Birello^{1,+}, Michele Re Fiorentin², Boxuan Wang¹,
Vittoria Colizza¹, and Eugenio Valdano^{1,*}.

¹*Sorbonne Université, INSERM, Institut Pierre Louis d'Epidémiologie et de Santé Publique, F75012, Paris, France.*

²*Department of Applied Science And Technology (DISAT), Politecnico di Torino, C.so Duca degli Abruzzi 24, 10129, Torino, Italy.*

⁺ *Department of Mathematical Sciences "Giuseppe Luigi Lagrange" (DISMA), Politecnico di Torino, C.so Duca degli Abruzzi 24, 10129, Torino, Italy.*

^{*} *Corresponding author eugenio.valdano@inserm.fr*

Abstract

An accurate and timely estimate of the reproduction ratio R of an infectious disease epidemic is crucial to make projections on its evolution and set up the appropriate public health response. Estimates of R routinely come from statistical inference on timelines of cases or their proxies like symptomatic cases, hospitalizations, deaths. Here, however, we prove that these estimates of R may not be accurate if the population is made up of spatially distinct communities, as the interplay between space and mobility may hide the true epidemic evolution from surveillance data. This means that surveillance may underestimate R over long periods, to the point of mistaking a growing epidemic for a subsiding one, misinforming public health response. To overcome this, we propose a correction to be applied to surveillance data that removes this bias and ensures an accurate estimate of R across all epidemic phases. We use COVID-19 as case study; our results, however, apply to any epidemic where mobility is a driver of circulation, including major challenges of the next decades: respiratory infections (influenza, SARS-CoV-2, emerging pathogens), vector-borne diseases (arboviruses). Our findings will help set up public health response to these threats, by improving epidemic monitoring and surveillance.

Main text

The reproduction ratio R is arguably the most used indicator to monitor the trend in the evolution of an infectious disease epidemic. R is the average number of secondary cases that each case generates: When it is larger than one, the epidemic wave is growing; when instead it is lower than one, it is subsiding [1, 2]. The reproduction ratio also measures the effectiveness of public health interventions, whose overarching goal is to bring an unconstrained epidemic ($R > 1$) below the epidemic threshold of $R = 1$: Accurately estimating the reproduction ratio is thus necessary to ascertain the current epidemic evolution, predict short-term trends, perform scenario analysis and plan public health action [3–7]. The standard way to measure R is to infer it from data coming from epidemiological surveillance [8–12]. These data may be timelines of detected cases or their proxies, like hospitalizations or deaths, and this approach applies to diseases spanning radically different epidemiology, transmission routes and burden, like influenza [13, 14], measles [15], COVID-19 [16], Ebola [17], cholera [18], dengue [19], malaria [20]. The resulting surveillance-based estimates of R are routinely used to design interventions [21]: Notwithstanding, we argue in this study that surveillance data may lead to biased estimates of the reproduction ratio in spatially structured populations, where geographically distinct communities (e.g., cities) are connected though human mobility. We will show that the complex interplay between spatial heterogeneities in transmissibility and the mixing network driven by human mobility hide the true dynamic structure of the epidemic process from population-level surveillance data. This mirrors the nature of most mathematical models of epidemic spread: they integrate space and spatial data at high resolution [22–27], but they find it harder to do the reverse, which is extracting high-resolution information from limited and coarse-grained surveillance data in the absence of knowledge of the underlying spatial dynamics is [28–30]. Crucially, this means that inference on surveillance data may either overestimate or underestimate it over long periods. This is of great public health relevance: measuring for instance a reproduction ratio below one when the true value is above would falsely signal that the epidemic is under control. Here, we study this bias, identify its origin and compute its magnitude. Then, we propose a correction to case incidence data that removes this bias and ensures that surveillance-based estimates of the reproduction ratio consistently give the true reproduction ratio of the epidemic. Our theoretical findings apply to any epidemic featuring relatively short generation time and for which mobility is a contributing factor in shaping its circulation within and across communities. This covers some of the global health threats that are being worst affected by climate change and demographic trends: viruses responsible for respiratory infections

– including SARS-CoV-2 and influenza – [31], vector-borne pathogens – including the arboviruses dengue, chikungunya, Zika [32, 33], and emergence events of new viruses or new viral strains [34]. To test and illustrate our findings, we use the French COVID-19 epidemic (see Fig. 1) before the advent of vaccination as a case study.

Theoretical formalism

The Galton–Watson branching process is a customary framework to model epidemic spread [35–37]. Let $I(0)$ be the initial number of cases, $I(1)$ the expected number of cases that the initial cases generate, and, generally, let $I(t)$ be the expected number of cases in the t -th generation. By definition of the reproduction ratio, we have that $I(t) = RI(t-1)$, which implies that $I(t) = R^t I(0)$. This equation means that the number of cases grows exponentially if $R > 1$. In any real outbreak other factors, like acquired immunity, seasonal effects or public-health interventions, will at some point curb this exponential growth by changing the value of R . Notwithstanding, we may assume R to be fairly constant either in the early phase of an outbreak, when those effects have not yet kicked in, or when the timescale at which immunity and mixing change is much longer than epidemic evolution [38, 39].

In the case of a population composed of N spatial communities, we may define the vector $\mathbf{I}(t) \in \mathbb{R}^N$, whose component $I(t)_i$ is the number of cases in generation t and community i . Likewise, the *reproduction operator* $\mathbf{R} \in \mathbb{R}^{N,N}$ encodes, in its component R_{ij} , the average number of cases generated among the residents of community i , by a case belonging to community j [40]. This definition of \mathbf{R} , and the results that we are going to derive from it, applies to any epidemic and disease. The specific parametrization of \mathbf{R} will instead depend on the specific transmission dynamics and natural history of the disease: for directly-transmitted diseases \mathbf{R} typically depends on mixing patterns among communities [41]; for vector-borne diseases the local abundance of the host vectors, modulating the effective transmissibility, needs to be factored in, too [32, 42]. The expected epidemic evolution then follows the equation

$$\mathbf{I}(t) = \mathbf{R}^t \mathbf{I}(0). \tag{1}$$

$\mathbf{I}(t)$ encodes both the total number of cases in the population in generation t and its spatial distribution. We define the former as the number $I_{tot}(t) = \sum_i I(t)_i$ and the latter as the vector $\mathbf{x}(t) \in \mathbb{R}^N$ whose components are $x(t)_i = I(t)_i / I_{tot}(t)$.

The reproduction ratio R of this process is the spectral radius of \mathbf{R} (i.e., the largest among the absolute values of its eigenvalues) [43], which is itself also a (nondegenerate)

eigenvalue, because \mathbf{R} is by definition nonnegative and can be assumed irreducible (see Supplementary Methods Section 1.3) so that the Perron-Frobenius theorem holds [44]. We also define \mathbf{v} as the Perron (right) eigenvector associated with R . \mathbf{v} is strictly positive ($v_i > 0$) and we normalize it so that $\sum_i v_i = 1$.

Measuring the true reproduction ratio of the system thus requires knowledge of the spectral structure of \mathbf{R} , i.e., of the spatial structure of the epidemic. Surveillance instead measures the reproduction ratio from the evolution of the incidence of infections or their proxies. This may happen globally, at the level of the entire population, or locally in each community. In our framework, the population-level observed reproduction ratio is $S(t) = I_{tot}(t+1)/I_{tot}(t)$, i.e., the generational growth rate. The local community-level observed reproduction ratio is instead $s_i(t) = I(t+1)_i/I(t)_i$.

A simple observation then underpins our study: in general $S(t)$ and $s_i(t)$ may be different from R , the spectral radius of \mathbf{R} , and, if that is the case, surveillance will not measure the true reproduction ratio.

To explore this, we will first determine the conditions leading to an unbiased measure of the reproduction ratio: $S(t) = R$.

When the true and observed reproduction ratios match

By virtue of the Perron-Frobenius theorem, $\mathbf{R}^t \rightarrow R^t \mathbf{v}\mathbf{v}^*$ asymptotically at large t , where \mathbf{v}^* is the dual of \mathbf{v} (easily computable as the left Perron eigenvector of \mathbf{R}) and normalized so that $\mathbf{v}^*\mathbf{v} = 1$. Asymptotically then equation (1) becomes $\mathbf{I}(t) \rightarrow [\mathbf{v}^*\mathbf{I}(0)] R^t \mathbf{v}$, which implies that $\mathbf{x}(t) \rightarrow \mathbf{v}$, $S(t) \rightarrow R$ and $s_i(t) \rightarrow R$. The epidemic dynamics thus brings the spatial distribution of cases toward \mathbf{v} , which we will refer to as the *equilibrium spatial distribution of infections*. Thus, for any epidemic dynamics, if cases are spatially distributed as the equilibrium distribution ($\mathbf{x} = \mathbf{v}$), then the error is zero and the true reproduction ratio is measured both globally ($S = R$) and locally $s_i = R$. Fig.1b shows evidence of the convergence to \mathbf{v} during the COVID-19 epidemic in France in late 2020 and early 2021. We used mobility data from Meta [45], a multinational technology company, to estimate \mathbf{R} for the 94 departments of mainland France, excluding Corsica (see Reconstruction of the reproduction operator from data). We reconstructed \mathbf{x} from surveillance data released by the French public health authority (see Supplementary Methods Section 1.1). In a period when \mathbf{R} was fairly constant (required by our formalism) the angle between \mathbf{x} and \mathbf{v} consistently decreased. Such angle, however, never got to zero because then \mathbf{R} changed, and, consistently, the equilibrium distribution \mathbf{v} changed. The description of the whole course of an epidemic wave indeed requires a time-varying \mathbf{R}

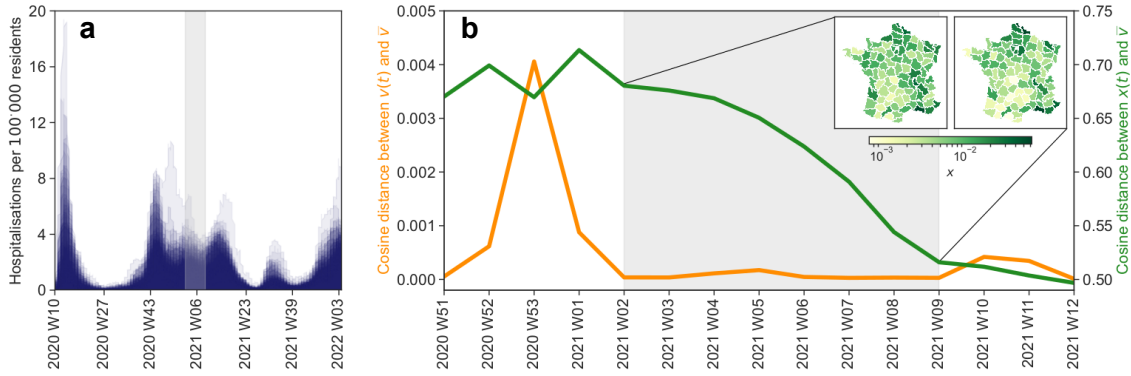


Fig.1|Convergence to the equilibrium spatial distribution of infections. **a**, The weekly number of new COVID-19-related hospitalizations per 100,000 residents is reported from week 10 of 2020 (Mar 2, 2020 to Jan 30, 2022). Each curve is that of one of the 94 departments (administrative level 2) of mainland France excluding the region of Corsica. The area in gray goes from week 2 to week 9 of 2021 (Jan 11 to Mar 7). **b**, The orange curve (left y axis) reports the weekly cosine distance between \mathbf{v} (computed from mobility data from that week - see Reconstruction of the reproduction operator from data) and its average ($\bar{\mathbf{v}}$) on the time interval in gray (the same as in **a**). The cosine distance between \mathbf{v} and $\bar{\mathbf{v}}$ is defined as $1 - \mathbf{v} \cdot \bar{\mathbf{v}} / (\|\mathbf{v}\| \|\bar{\mathbf{v}}\|)$. The green curve (right y axis) reports the cosine distance between $\bar{\mathbf{v}}$ and the weekly spatial distribution of COVID-19 cases \mathbf{x} in French departments reconstructed from hospitalizations - details in Supplementary Methods Section 1.1. The two inset maps show the spatial distribution \mathbf{x} in week 2 and week 9 of 2021, respectively (edges of the time interval in gray).

and that is beyond the scope of this study. Locally in time, however, in periods during which \mathbf{R} is fairly constant, the system will evolve towards the equilibrium distribution determined by the Perron eigenvector of \mathbf{R} at that time.

But there exists a class of operators \mathbf{R} for which the error is globally zero even out of equilibrium ($\mathbf{x} \neq \mathbf{v}$). First, let us rewrite the observed reproduction ratio in matrix form as

$$S(t) = \frac{I_{tot}(t+1)}{I_{tot}(t)} = \mathbf{F}^T \mathbf{R} \mathbf{x}(t), \quad (2)$$

where we introduced \mathbf{F} as the unit column vector ($F_i = 1 \forall i$). If we assume that $\mathbf{v}^* = \mathbf{F}^T$ ($v_i^* = 1$) then we can apply \mathbf{R} leftwards in equation (2) and get $S(t) = R$ at any time and for any spatial distribution \mathbf{x} . Now, the requirement $\mathbf{v}^* = \mathbf{F}^T$ imposes that \mathbf{R} is proportional to a left-stochastic matrix: indeed $\mathbf{F}^T \mathbf{R} = R \mathbf{F}^T$ means $\sum_j R_{ji} = R$, so that each column sums to R . $r_i \equiv \sum_j R_{ji}$ is by definition the expected number of secondary cases generated by a case resident of i regardless of where they are generated. If r_i is constant, every case, anywhere, has the same overall *transmission potential*: $r_i = R \forall i$. If this is the case, the observed reproduction ratio is unbiased regardless of the spatial epidemic coupling among communities. This implies that only the combination of spatial epidemic coupling and spatial heterogeneity in transmission potential may cause a

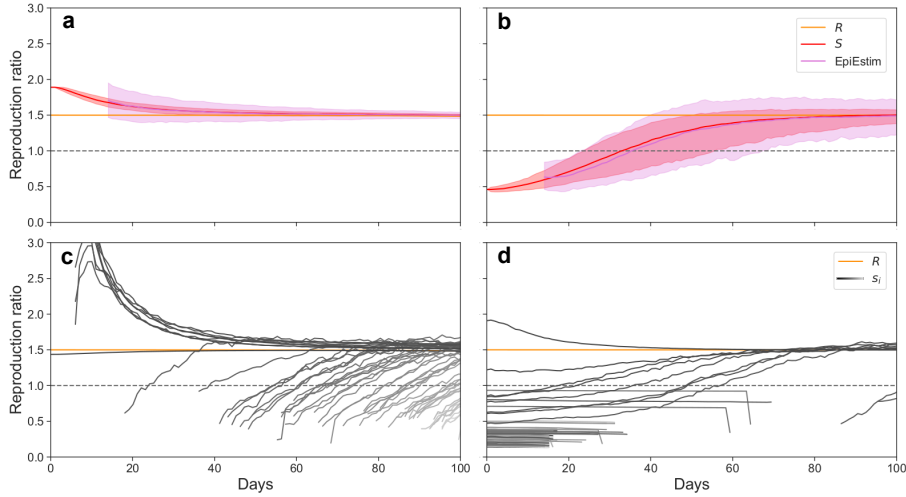


Fig.2|Comparison of the true and measured reproduction ratios. We generated stochastic simulations of a COVID-19-like epidemic in France using a metapopulation model, whereby we divided the French population in 94 spatial communities corresponding to the department of mainland France minus Corsica, and modeled within- and between-community mixing using mobility data by Meta. See Epidemic simulations for details on how we built \mathbf{R} from mobility data and on the epidemic spread model. R (yellow) is the true reproduction ratio, S (red) is the observed reproduction ratio as described in the paper, s_i are the locally observed reproduction ratios, and $EpiEstim$ (purple) is the reproduction ratio computed from incidence data using the *EpiEstim* package [11] (see Supplementary Methods Section 1.4 for details). Two initial conditions are tested: in **a** and **c** 100 initial cases are seeded in the department of Paris, while in **b** and **d** 100 initial cases are seeded among departments proportionally to their population. We run 1000 runs of the stochastic model, and plot medians with solid lines and 95% confidence intervals with shaded areas. For the s_i , confidence intervals are omitted for readability.

global difference between the observed and the true reproduction ratios. Notably, locally-measured reproduction ratios may instead differ from R even in the case $\mathbf{v}^* = \mathbf{F}^T$.

When the true and observed reproduction ratios do not match

We now focus on the out-of-equilibrium dynamics ($\mathbf{x}(t) \neq \mathbf{v}$) and measure the bias in the estimate of R as the relative difference between the observed and the true reproduction ratios

$$\Delta(t) = \frac{S(t) - R}{R}. \quad (3)$$

We call Λ_α ($\alpha = 1, \dots, N - 1$) the (possibly degenerate) eigenvalues of \mathbf{R} other than R and, by Perron-Frobenius theorem, $|\Lambda_\alpha| < R$. With calculations reported in Calculation

of $\Delta(t)$: proof of equation (4), we find that

$$\Delta(t) = C(t) \sum_{\alpha} z_{\alpha} \left(1 - \frac{\Lambda_{\alpha}}{R}\right) \left(\frac{\Lambda_{\alpha}}{R}\right)^t, \quad (4)$$

where $C(t)$ is positive and asymptotically constant, and z_{α} is a (possibly complex) number proportional to the scalar product between \mathbf{F} and the projection of the initial condition $\mathbf{x}(0)$ on the α -th mode. The modes in equation (4) for which $\Lambda_{\alpha} \approx R$, or that are almost orthogonal to the initial configuration $\mathbf{x}(0)$, are suppressed from the start and do not bias the estimate of the reproduction ratio. The other modes, instead, possibly bias the reproduction ratio with an effect that becomes smaller as the epidemic evolves, with a characteristic decay time $\tau_{\alpha} = 1/\log(R/|\Lambda_{\alpha}|)$. In addition, those modes for which Λ_{α} is not real and positive have an oscillating term. Specifically, if Λ_{α} has a nonzero imaginary part, then its complex conjugate is also an eigenvalue and their combined contribution oscillates with period $T_{\alpha} = 2\pi/|\theta_{\alpha}|$, where $\theta_{\alpha} = \arg \Lambda_{\alpha}$ (with $\theta_{\alpha} \in (-\pi, \pi]$). This also holds for negative eigenvalues ($\theta_{\alpha} = \pi$) – see Calculation of $\Delta(t)$: proof of equation (4) for a detailed calculation. These modes with $\theta_{\alpha} \neq 0$ will induce visible oscillations in $\Delta(t)$ if they oscillate faster than their characteristic decay time. We can quantify this by requiring the oscillation period to be smaller than the decay time: $T_{\alpha} \leq \tau_{\alpha}$. This gives the inequality

$$\frac{|\Lambda_{\alpha}|}{R} \geq e^{-\frac{|\theta_{\alpha}|}{2\pi}} \geq e^{-\frac{1}{2}} \approx 0.61, \quad (5)$$

where the lower bound in equation (5) occurs when Λ_{α} is real and negative ($\theta_{\alpha} = \pi$).

To test the predictions of our theory in a realistic scenario, we considered again the COVID-19 epidemic in France and built a stochastic metapopulation model using the same mobility data as in Fig. 1b. The details of the model are reported in Epidemic simulations. We measured the true and the observed reproduction ratios, reported in Fig. 2, which shows that surveillance-based estimates may remain consistently biased for a long period and, depending on where the epidemic wave started (initial conditions), they may either overestimate or underestimate the true reproduction ratio. The case depicted in Fig. 2b is particularly concerning: during the first month of the simulated epidemic, surveillance records a lower-than-one reproduction ratio which would mistakenly point to a subsiding outbreak. In reality, the true reproduction ratio is fixed to well above one, and only after two months of simulated epidemic does the surveillance based estimate reach the true value. Alongside the estimate of S given within the framework of the Galton-Watson process (equation (2)), in Fig. 2a,b we also provide an estimate of the observed reproduction ratio by feeding incident cases to the library *EpiEstim* [11], one of the most popular tools to compute the reproduction ratio from surveillance data. The fact that the

two measures overlap confirms that the Galton-Watson process correctly reproduces the phenomenology under study even in realistic scenarios. Notwithstanding, more detailed frameworks [43, 46, 47] could be used to study the impact of heterogeneous generation intervals.

Finally, Fig. 2c and Fig. 2d show that locally measured reproduction ratios converge to the true value at different times and with different speeds, and that, at the same moment in time, some communities may overestimate R and some underestimate it. This last point can actually be proven to be always the case. The Collatz-Wielandt inequalities tell us that, for any spatial distribution of cases \mathbf{x} , $\min_{i|x_i \neq 0} (\mathbf{R}\mathbf{x})_i/x_i \leq R$ and $\max_{i|x_i \neq 0} (\mathbf{R}\mathbf{x})_i/x_i \geq R$. Given that $s_i = (\mathbf{R}\mathbf{x})_i/x_i$, out of equilibrium there will always be at least one community overestimating the true reproduction ratio ($s_i > R$) and one underestimating it ($s_i < R$).

Fig. 2 shows no oscillations in the sign of $\Delta(t)$, compatible with the fact that the operator \mathbf{R} we built from mobility data has only real and positive eigenvalues. We extended our analysis to 32 European countries: 24 members of the European Union (excluding Cyprus, Ireland and Latvia for lack of data) plus Albania, Bosnia and Hercegovina, Iceland, Montenegro, Norway, Serbia, Sweden, UK - see details in Supplementary Figure 1. For all of them we built the operator \mathbf{R} using colocation and population data at the admin-2 level, similarly to what we did for France. We found at least one real, negative eigenvalue in 11 out of 32 countries, but nowhere did they cause visible oscillations, as the oscillation period was always larger than twice the decay time. We did not find non-real eigenvalues. This begs the question whether oscillations are actually observable in real systems. To rigorously determine the conditions for a specific spectrum in a generic nonnegative matrix is not possible, except for specific or low-dimensional cases [48]. We can, however, plausibly associate the presence of an oscillating mode with period T_α to the existence of a cycle of approximate length T_α in the (weighted, directed) network which has \mathbf{R} as its adjacency matrix [49, 50]. Slow oscillations (large T_α) would then require the presence of long cycles in \mathbf{R} , which are unlikely to be generated by the recurrent mobility patterns that drive the spatial spread of epidemic outbreaks following pathogen importation [26, 51]. Fast oscillations, and in particular those generated by real, negative eigenvalues, may instead be more common. They would require epidemics that are strongly coupled, i.e., where pairs of communities exist in which infected residents generate, on average, more cases in the other community than in their own, but this is not the case in the countries we examined and for the spatial resolution we considered.

In the absence of oscillations, the observed reproduction ratio consistently either overestimates or underestimates the true reproduction ratio, as $\Delta(t)$ decays to zero without

ever changing sign. In this case, we can determine the sign of the bias from the initial condition: $\Delta(0) = \sum_j r_j x(0)_j - R$. By the Perron-Frobenius theorem, j_{min}, j_{max} exist so that $r_{j_{min}} \leq R$ and $r_{j_{max}} \geq R$. Thus, the initial location of cases will completely determine the sign of the error that surveillance will make. If the epidemic starts j_{max} – or in general in communities with high transmission potential –, surveillance will consistently overestimate the true reproduction ratio until the bias decays to zero. Conversely, if it starts in j_{min} – or in communities with low transmission potential –, surveillance will underestimate R .

Correction to surveillance data

So far we have proven that surveillance-based estimates of the reproduction ratio may be biased. We will now propose a way to correct for this bias. Equation (2) computes, within our simplified model, the reproduction ratio in terms of the overall observed incidence of cases $I_{tot}(t)$. This can also be trivially interpreted as proportional to the unweighted average of the incidence across communities: $I_{tot}(t) = N (\sum_i I_i(t)/N)$. From this, we define a new modified incidence using an average weighted by the entries of the Perron dual vector:

$$I_{tot}^{(v)}(t) = N \left(\frac{\sum_i v_i^* I_i(t)}{\sum_i v_i^*} \right) = N \sum_i v_i^* I_i(t) = N \mathbf{v}^* \mathbf{I}(t). \quad (6)$$

We now define a new modified observed reproduction ratio using the modified incidence ($I_{tot}^{(v)}(t)$) – compare this with equation (2):

$$S^{(v)}(t) = \frac{I_{tot}^{(v)}(t+1)}{I_{tot}^{(v)}(t)} = \frac{\mathbf{v}^* \mathbf{I}(t+1)}{\mathbf{v}^* \mathbf{I}(t)} = \frac{\mathbf{v}^* \mathbf{R} \mathbf{I}(t)}{\mathbf{v}^* \mathbf{I}(t)} = R \frac{\mathbf{v}^* \mathbf{I}(t)}{\mathbf{v}^* \mathbf{I}(t)} = R. \quad (7)$$

The practical advantage for epidemic monitoring is clear: our correction gives an unbiased estimate of the reproduction ratio from surveillance data all along the epidemic wave, unlike traditional measures. It has, however, two potential drawbacks. The former is that if the initial epidemic seeding occurs in communities where v_i^* is small, then $\mathbf{v}^* \mathbf{I}(t)$ will be very small: stochastic fluctuations would then cause large changes in $S^{(v)}$. In that case then $S^{(v)}$ may well be accurate, but not precise. Luckily, however, no initial condition can be orthogonal to \mathbf{v}^* whose entries are strictly positive, so even if $\mathbf{v}^* \mathbf{x}$ is initially small, it is likely to increase quickly and with it the precision of the measurement. In Fig. 3 we show that $S^{(v)}$ accurately measures the true reproduction ratio from the beginning of the epidemic wave, in the case of the simulated epidemics of Fig. 2. Notably,

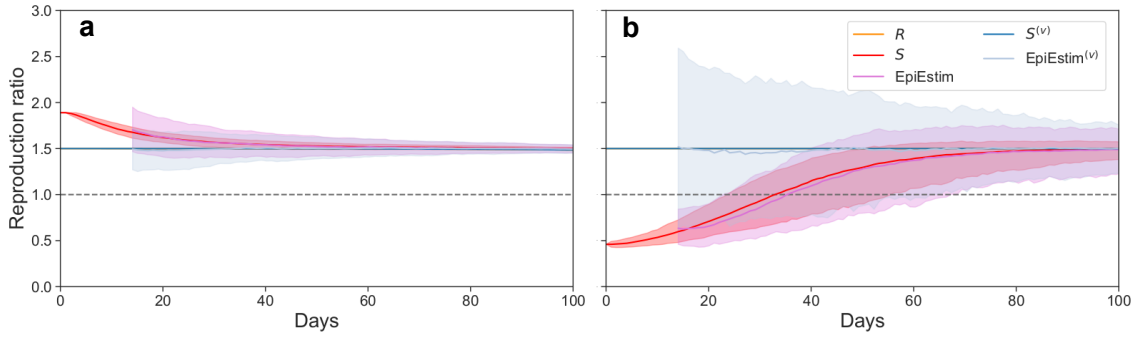


Fig.3|Corrected reproduction ratio. This figure uses the same stochastic epidemic model as in Fig. 2 and the same initial conditions, *i.e.*, panels **a** and **b** correspond to panels **a** and **b** in Fig.2 respectively. Medians and 95% confidence intervals are computed and shown over 1000 runs. We compare the standard reproduction ratio measured from surveillance data – both in the Galton-Watson formalism (red) and with *EpiEstim* (purple) on incidence data – and the corresponding \mathbf{v}^* -corrected estimates: Galton-Watson formalism (blue) and with *EpiEstim* (light blue) on modified incidence data $I_{tot}^{(v)}$.

Fig. 3 also shows that if you feed $I_{tot}^{(v)}(t)$ to *EpiEstim* instead of $I_{tot}(t)$ you will also completely remove the bias on the estimate of the reproduction ratio. Our proposed modified incidence can then be readily incorporated to standard tools for public health surveillance, to improve their accuracy.

The latter potential drawback is that our correction requires knowing \mathbf{v}^* . We argue, however, that this does not require knowing or measuring \mathbf{R} in real time (from which R could then be directly measured) and that a good estimate of \mathbf{v}^* for epidemic monitoring can be computed during *peace time*, from past population and mobility data (pre-epidemic, or from data collected during earlier epidemic phases). Indeed \mathbf{v}^* is more stable than \mathbf{R} for the fact that any change happening homogeneously across communities (e.g., changes in the rate of immunity, public health interventions) would change the latter, not the former. Fig. 4 compares the standard observed reproduction ratio of COVID-19 in France between late 2020 and March 2021 to our correction. The former is computed with *EpiEstim* on inferred case incidence, the latter is computed with *EpiEstim* on the corrected incidence $I_{tot}^{(v)}$, with \mathbf{v}^* computed from past mobility data. Notably, we tested different choices of \mathbf{v}^* going back up to August 2020, *i.e.*, five months prior to the period under study, which confirms that our correction is robust to using past mobility data to reconstruct \mathbf{v}^* . Our correction seems to point to the fact that traditional surveillance underestimated the true reproduction ratio of COVID-19 in France during January and February 2021. This underestimation is even more consequential because surveillance recorded a lower-than-one reproduction ratio during more than two weeks (see also official reports from that time [52]), indicating a subsiding epidemic wave. This is at odds

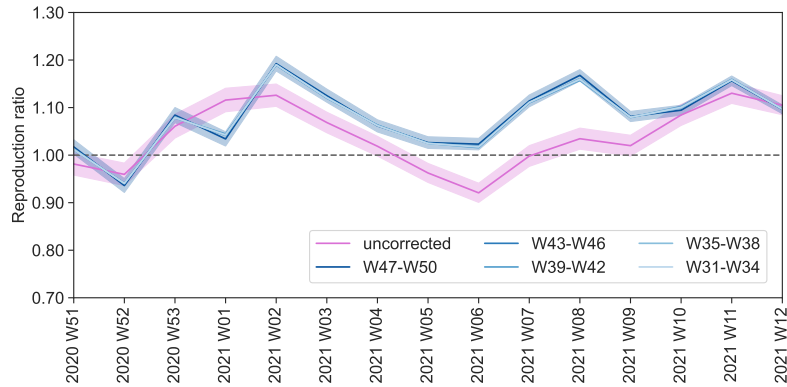


Fig.4|Application of the proposed correction to COVID-19 data in France. The pink curve reports the reproduction ratio of COVID-19 in France obtained from country-level incidence of cases, in the same time interval as in Fig. 1b, using the package *EpiEstim*. The blue curves reports the corrected reproduction ratio obtained by feeding *EpiEstim* the corrected incidence as in Eq. (6). For this, the Perron dual vector \mathbf{v}^* is reconstructed from mobility data at different times prior the observation period, specified in the legend as week ranges of year 2020. The shaded areas are the 95% credibility intervals computed by *EpiEstim*. For readability, only those of the pink curve and the darkest blue curve are shown. The different blue curves are hardly distinguishable because they overlap. See Reconstruction of the reproduction operator from data for a detailed explanation on how to compute \mathbf{v}^* from data.

with what we know happened: a growing epidemic wave – the French *third wave* – that led to a national lockdown, enforced on April 3 2021, i.e., immediately after the time window depicted in Fig. 4. Our corrected reproduction ratio would have instead consistently signaled a growing epidemic wave throughout the first three months of 2021. This discrepancy carries great significance when put into the context of the debate over public health response at that time. In early 2021 a national curfew was in effect but cases were rising due to the introduction and gradual takeover of the Alpha variant of SARS-CoV-2. Authorities were wary of additional restrictions and were relying on mass vaccination despite models suggesting that it might not be enough [53] – only 3% of the population had received at least one dose by mid February [52] (week 6 of 2021 in Fig. 4). It is conceivable, albeit circumstantial, that the fact that surveillance underestimated the severity of the wave could have contributed to delaying the enforcement of stricter movement restrictions, which became anyway inevitable later in April.

Our study describes a practicable way to improve the accuracy of the information that flows from epidemiological surveillance to public health policymakers. And better information may lead to more effective policies for preventing and controlling epidemic threats.

Methods

Calculation of $\Delta(t)$: proof of equation (4)

Combining equation (1) and equation (2) we get the time evolution of the observed reproduction ratio:

$$S(t) = \frac{\mathbf{F}^T \mathbf{R}^{t+1} \mathbf{x}(0)}{\mathbf{F}^T \mathbf{R}^t \mathbf{x}(0)}. \quad (8)$$

We insert this into equation (3) and get

$$\Delta(t) = \frac{1}{R} \frac{\mathbf{F}^T (\mathbf{R} - R) \mathbf{R}^t \mathbf{x}(0)}{\mathbf{F}^T \mathbf{R}^t \mathbf{x}(0)}. \quad (9)$$

We introduce the eigenvectors of \mathbf{R} (other than \mathbf{v}): \mathbf{w}_α eigenvector with corresponding eigenvalue Λ_α . Analogously we define the corresponding dual vector \mathbf{w}_α^* . Then, we decompose \mathbf{F}^T in the dual basis: $\mathbf{F}^T = \mathbf{v}^* + \sum_\alpha (\mathbf{F}^T \mathbf{w}_\alpha) \mathbf{w}_\alpha^*$. Using this decomposition in equation (9) and applying \mathbf{R} leftwards on the dual eigenvectors we get

$$\Delta(t) = - \frac{\mathbf{F}^T \left[\sum_\alpha \left(\frac{\Lambda_\alpha}{R} \right)^t \left(1 - \frac{\Lambda_\alpha}{R} \right) \mathbf{w}_\alpha \mathbf{w}_\alpha^* \right] \mathbf{x}(0)}{\mathbf{F}^T \left[\mathbf{v} \mathbf{v}^* + \sum_\alpha \left(\frac{\Lambda_\alpha}{R} \right)^t \mathbf{w}_\alpha \mathbf{w}_\alpha^* \right] \mathbf{x}(0)}. \quad (10)$$

The denominator is $C(t)$ in equation (4):

$$C(t) = \frac{1}{\mathbf{F}^T \left[\mathbf{v} \mathbf{v}^* + \sum_\alpha \left(\frac{\Lambda_\alpha}{R} \right)^t \mathbf{w}_\alpha \mathbf{w}_\alpha^* \right] \mathbf{x}(0)}. \quad (11)$$

$C(t)$ is always strictly positive because it is proportional to $\mathbf{F}^T \mathbf{R}^t \mathbf{x}(0)$ and tends to $\mathbf{v}^* \mathbf{x}(0)$, i.e., the component of the initial condition onto the eigenspace of the Perron eigenvalue. This component is always nonzero because no $\mathbf{x}(0)$ is nonnegative (as it is a spatial distribution of cases) and no nonnegative vector can be orthogonal to a strictly positive vector. It is thus the numerator which gives the trend and sign of $\Delta(t)$. Equation (10) then gives the value of the factors z_α in equation (4):

$$z_\alpha = -\mathbf{F}^T (\mathbf{w}_\alpha \mathbf{w}_\alpha^*) \mathbf{x}(0) \quad (12)$$

In the case of degenerate eigenvalue one should simply replace $\mathbf{w}_\alpha \mathbf{w}_\alpha^*$ with the appropriate projector over the whole eigenspace. Note that, as discussed before, the denominator in equation (10) is always real and positive so any complex phase of z_α must arise from Λ_α and $\mathbf{w}_\alpha \mathbf{w}_\alpha^*$.

Calculation of $\Delta(t)$: τ_α, T_α

We isolate in equation (4) the contribution of each mode $M_\alpha(t)$: $\Delta(t) = \sum_\alpha M_\alpha(t)$, where

$$M_\alpha(t) = M_\alpha(0) \left(\frac{\Lambda_\alpha}{R} \right)^t = M_\alpha(0) \left(\frac{|\Lambda_\alpha|}{R} \right)^t e^{i\theta_\alpha t} = M_\alpha(0) e^{-t/\tau_\alpha} e^{i\theta_\alpha t}, \quad (13)$$

where we used the definition of τ_α given in the main text. The decaying term with characteristic time τ_α is visible.

If Λ_α is real and positive then $\theta_\alpha = 0$ and the oscillating term vanishes. If Λ_α is real and negative then $\theta_\alpha = \pi$ and the oscillating term becomes an alternating sign: $e^{i\theta_\alpha t} = (-1)^t$. This is an oscillation with period $T_\alpha = 2$, which is compatible with the definition of T_α given in the main text. Finally, if $\Lambda_\alpha \notin \mathbb{R}$, then $\bar{\Lambda}_\alpha$ is also an eigenvalue, where the bar denotes complex conjugation. We will call $\bar{\alpha}$ the index corresponding to that eigenvalue: $\Lambda_{\bar{\alpha}} = \bar{\Lambda}_\alpha$. Also, the projector over the eigenspace of $\Lambda_{\bar{\alpha}}$ is the elementwise complex conjugate of the projector over the eigenspace of Λ_α , meaning that $z_{\bar{\alpha}} = \bar{z}_\alpha$, and thus $M_{\bar{\alpha}} = \bar{M}_\alpha(0)$. Then $\alpha, \bar{\alpha}$ contribute in pair, as follows:

$$\begin{aligned} M_\alpha(t) + M_{\bar{\alpha}}(t) &= e^{-t/\tau_\alpha} [M_\alpha(0)e^{i\theta_\alpha t} + M_{\bar{\alpha}}(0)e^{-i\theta_\alpha t}] \\ &= 2e^{-t/\tau_\alpha} |M_\alpha(0)| \operatorname{Re} e^{i\theta_\alpha t + \phi_\alpha} = 2e^{-t/\tau_\alpha} \cos\left(\frac{2\pi}{T_\alpha}t + \phi_\alpha\right). \end{aligned} \quad (14)$$

Here we used the definition of T_α given in the main text, explicitly showing the emergence of the oscillating term with period T_α .

Reconstruction of the reproduction operator from data

The main data used for the reconstruction of reproduction operators for mainland France are Meta Colocation Maps[45]. They give the probability p_{ij} that a randomly chosen person that is resident of community i and a randomly chosen person resident of community j are both located in a same $600m \times 600m$ square, during a randomly chosen five-minutes time window, in a given week. Note that diagonal elements p_{ii} quantify the mixing within each community. From these diagonal probabilities we discounted spurious co-location time due to people staying at home in spatially contiguous dwellings using Movement Range Maps (see Data availability and Supplementary Methods Section 1.2). The data were provided at the resolution of departments (ADM 2). To reconstruct \mathbf{R} from these data, we assumed that the expected number of secondary cases generated among the residents of community i , by a case who is resident of community j , is given

by $R_{ij} = Cp_{ij}n_i$, where n_i is the population of spatial patch i , and C is an overall transmissibility parameter. Notably, while the value of the spectral radius of \mathbf{R} clearly depends on C , the left and right Perron eigenvectors \mathbf{v} and \mathbf{v}^* do not, and depend solely on the data.

Epidemic simulations

The model of epidemic spread used in simulations is a stochastic discrete-time metapopulation model whereby spatially distinct communities are linked through mobility [26, 27, 54, 55]. We use a synthetic population based on census data from the National Institute of Statistics and Economic Studies (INSEE) in France. We divide this population in 94 spatial communities corresponding to the departments of mainland France except Corsica. Meta Colocation Maps [45] and Movement Range Maps are used to reconstruct the coupling p_{ij} between communities i and j and the within-community i mixing p_{ii} . We use a compartmental model of COVID-19 from [56]. We compute the reproduction ratio for our model according to the next generation method [57], obtaining:

$$R = \rho(K) \frac{\beta}{\mu} (1 - p_{sc} + \beta_I p_{sc}), \quad (15)$$

where $\rho(K)$ is the spectral radius of the matrix $K_{ij} = p_{ij}n_i$, n_i is the population of community i , μ is the recovery rate, p_{sc} is the probability of sub-clinical infections and β_I is the factor by which the transmissibility of sub-clinical cases is reduced (see [56]). The other parameters are also taken from [56], and the overall transmission rate β is set so that $R = 1.5$.

Data availability

Meta Colocation Maps and Meta Movement Range Maps, which were used to reconstruct reproduction operators and to infer between- and within-community mixing for stochastic simulations can be requested at <https://dataforgood.facebook.com/dfg/tools/colocation-maps> and <https://dataforgood.facebook.com/dfg/tools/movement-range-maps> respectively. Hospital admission data in France are available at <https://www.data.gouv.fr>. French census data can be found at <https://www.insee.fr>. All websites accessed June 2023.

Acknowledgements

Colocation data were available thanks to *Data For Good at Meta*.

References

1. Keeling, M. J. & Rohani, P. *Modeling Infectious Diseases in Humans and Animals* ISBN: 978-0-691-11617-4 (Princeton University Press, Princeton, NJ, USA, 2007).
2. Nishiura, H. & Chowell, G. en. in *Mathematical and Statistical Estimation Approaches in Epidemiology* (eds Chowell, G., Hyman, J. M., Bettencourt, L. M. A. & Castillo-Chavez, C.) 103–121 (Springer Netherlands, Dordrecht, 2009). ISBN: 978-90-481-2313-1.
3. Wallinga, J., van Boven, M. & Lipsitch, M. Optimizing infectious disease interventions during an emerging epidemic. *Proceedings of the National Academy of Sciences* **107**. Publisher: Proceedings of the National Academy of Sciences, 923–928 (Jan. 2010).
4. Ridenhour, B., Kowalik, J. M. & Shay, D. K. Unraveling R0: Considerations for Public Health Applications. *American Journal of Public Health* **108**, S445–S454. ISSN: 0090-0036 (Dec. 2018).
5. Thompson, R. N., Gilligan, C. A. & Cunniffe, N. J. Control fast or control smart: When should invading pathogens be controlled? en. *PLOS Computational Biology* **14**. Publisher: Public Library of Science, e1006014. ISSN: 1553-7358 (Feb. 2018).
6. Dhillon, R. S., Srikrishna, D. & Chowell, G. Getting to zero in the DR Congo Ebola outbreak. English. *The Lancet Infectious Diseases* **20**. Publisher: Elsevier, 395–397. ISSN: 1473-3099, 1474-4457 (Apr. 2020).
7. Pan, A. *et al.* Association of Public Health Interventions With the Epidemiology of the COVID-19 Outbreak in Wuhan, China. *JAMA* **323**, 1915–1923. ISSN: 0098-7484 (May 2020).
8. Wallinga, J. & Lipsitch, M. How generation intervals shape the relationship between growth rates and reproductive numbers. *Proceedings of the Royal Society B: Biological Sciences* **274**, 599–604. ISSN: 0962-8452 (Feb. 2007).
9. Davoudi, B. *et al.* Early Real-Time Estimation of the Basic Reproduction Number of Emerging Infectious Diseases. *Physical Review X* **2**. Publisher: American Physical Society, 031005 (July 2012).
10. Obadia, T., Haneef, R. & Boëlle, P.-Y. The R0 package: a toolbox to estimate reproduction numbers for epidemic outbreaks. *BMC Medical Informatics and Decision Making* **12**, 147. ISSN: 1472-6947 (Dec. 2012).

-
11. Cori, A., Ferguson, N. M., Fraser, C. & Cauchemez, S. A New Framework and Software to Estimate Time-Varying Reproduction Numbers During Epidemics. *American Journal of Epidemiology* **178**, 1505–1512. ISSN: 0002-9262 (Nov. 2013).
 12. Thompson, R. N. *et al.* Improved inference of time-varying reproduction numbers during infectious disease outbreaks. en. *Epidemics* **29**, 100356. ISSN: 1755-4365 (Dec. 2019).
 13. Biggerstaff, M., Cauchemez, S., Reed, C., Gambhir, M. & Finelli, L. Estimates of the reproduction number for seasonal, pandemic, and zoonotic influenza: a systematic review of the literature. *BMC Infectious Diseases* **14**, 480. ISSN: 1471-2334 (Sept. 2014).
 14. Thompson, R., Wood, J. G., Tempia, S. & Muscatello, D. J. Global variation in early epidemic growth rates and reproduction number of seasonal influenza. en. *International Journal of Infectious Diseases* **122**, 382–388. ISSN: 1201-9712 (Sept. 2022).
 15. Guerra, F. M. *et al.* The basic reproduction number (R₀) of measles: a systematic review. English. *The Lancet Infectious Diseases* **17**. Publisher: Elsevier, e420–e428. ISSN: 1473-3099, 1474-4457 (Dec. 2017).
 16. Li, Y. *et al.* The temporal association of introducing and lifting non-pharmaceutical interventions with the time-varying reproduction number (R) of SARS-CoV-2: a modelling study across 131 countries. English. *The Lancet Infectious Diseases* **21**. Publisher: Elsevier, 193–202. ISSN: 1473-3099, 1474-4457 (Feb. 2021).
 17. Maganga, G. D. *et al.* Ebola Virus Disease in the Democratic Republic of Congo. *New England Journal of Medicine* **371**. Publisher: Massachusetts Medical Society, 2083–2091. ISSN: 0028-4793 (Nov. 2014).
 18. Mukandavire, Z. *et al.* Estimating the reproductive numbers for the 2008–2009 cholera outbreaks in Zimbabwe. en. *Proceedings of the National Academy of Sciences* **108**, 8767–8772. ISSN: 0027-8424, 1091-6490 (May 2011).
 19. Codeço, C. T., Villela, D. A. M. & Coelho, F. C. Estimating the effective reproduction number of dengue considering temperature-dependent generation intervals. en. *Epidemics* **25**, 101–111. ISSN: 1755-4365 (Dec. 2018).
 20. Routledge, I. *et al.* Estimating spatiotemporally varying malaria reproduction numbers in a near elimination setting. en. *Nature Communications* **9**. Number: 1 Publisher: Nature Publishing Group, 2476. ISSN: 2041-1723 (June 2018).
 21. *Introducing a coherent European framework for tuning COVID-19 response measures* en. Mar. 2021.
-

-
22. Hufnagel, L., Brockmann, D. & Geisel, T. Forecast and control of epidemics in a globalized world. *Proceedings of the National Academy of Sciences* **101**. Publisher: Proceedings of the National Academy of Sciences, 15124–15129 (Oct. 2004).
 23. Balcan, D. & Vespignani, A. Phase transitions in contagion processes mediated by recurrent mobility patterns. en. *Nature Physics* **7**. Number: 7 Publisher: Nature Publishing Group, 581–586. ISSN: 1745-2481 (July 2011).
 24. Pastor-Satorras, R., Castellano, C., Van Mieghem, P. & Vespignani, A. Epidemic processes in complex networks. *Reviews of Modern Physics* **87**, 925–979. ISSN: 15390756 (2015).
 25. Soriano-Paños, D., Lotero, L., Arenas, A. & Gómez-Gardeñes, J. Spreading Processes in Multiplex Metapopulations Containing Different Mobility Networks. *Physical Review X* **8**. Publisher: American Physical Society, 031039 (Aug. 2018).
 26. Gómez-Gardeñes, J., Soriano-Paños, D. & Arenas, A. Critical regimes driven by recurrent mobility patterns of reaction–diffusion processes in networks. en. *Nature Physics* **14**. Number: 4 Publisher: Nature Publishing Group, 391–395. ISSN: 1745-2481 (Apr. 2018).
 27. Chang, S. *et al.* Mobility network models of COVID-19 explain inequities and inform reopening. en. *Nature* **589**. Publisher: Nature Publishing Group, 82–87. ISSN: 1476-4687 (Nov. 2020).
 28. Coletti, P., Poletto, C., Turbelin, C., Blanchon, T. & Colizza, V. Shifting patterns of seasonal influenza epidemics. en. *Scientific Reports* **8**. Number: 1 Publisher: Nature Publishing Group, 12786. ISSN: 2045-2322 (Aug. 2018).
 29. Scarpino, S. V. & Petri, G. On the predictability of infectious disease outbreaks. en. *Nature Communications* **10**. Number: 1 Publisher: Nature Publishing Group, 898. ISSN: 2041-1723 (Feb. 2019).
 30. Castro, M., Ares, S., Cuesta, J. A. & Manrubia, S. The turning point and end of an expanding epidemic cannot be precisely forecast. en. *Proceedings of the National Academy of Sciences* **117**. Publisher: National Academy of Sciences Section: Biological Sciences, 26190–26196. ISSN: 0027-8424, 1091-6490 (Oct. 2020).
 31. Li, Y. & Nair, H. Trends in the global burden of lower respiratory infections: the knowns and the unknowns. English. *The Lancet Infectious Diseases* **22**. Publisher: Elsevier, 1523–1525. ISSN: 1473-3099, 1474-4457 (Nov. 2022).

-
32. Messina, J. P. *et al.* The current and future global distribution and population at risk of dengue. en. *Nature Microbiology* **4**. Number: 9 Publisher: Nature Publishing Group, 1508–1515. ISSN: 2058-5276 (Sept. 2019).
 33. Romanello, M. *et al.* The 2022 report of the Lancet Countdown on health and climate change: health at the mercy of fossil fuels. English. *The Lancet* **400**. Publisher: Elsevier, 1619–1654. ISSN: 0140-6736, 1474-547X (Nov. 2022).
 34. Carlson, C. J. *et al.* Climate change increases cross-species viral transmission risk. en. *Nature* **607**. Number: 7919 Publisher: Nature Publishing Group, 555–562. ISSN: 1476-4687 (July 2022).
 35. Watson, H. W. & Galton, F. On the Probability of the Extinction of Families. *The Journal of the Anthropological Institute of Great Britain and Ireland* **4**, 138–144. ISSN: 09595295 (1875).
 36. Lloyd-Smith, J. O., Schreiber, S. J., Kopp, P. E. & Getz, W. M. Superspreading and the effect of individual variation on disease emergence. en. *Nature* **438**. Number: 7066 Publisher: Nature Publishing Group, 355–359. ISSN: 1476-4687 (Nov. 2005).
 37. Hellewell, J. *et al.* Feasibility of controlling COVID-19 outbreaks by isolation of cases and contacts. en. *The Lancet Global Health* **8**, e488–e496. ISSN: 2214-109X (Apr. 2020).
 38. Kucharski, A. J. *et al.* Effectiveness of ring vaccination as control strategy for Ebola virus disease. *Emerging infectious diseases* **22**, 105 (2016).
 39. De Meijere, G. *et al.* Attitudes towards booster, testing and isolation, and their impact on COVID-19 response in winter 2022/2023 in France, Belgium, and Italy: a cross-sectional survey and modelling study. en. *The Lancet Regional Health - Europe* **28**, 100614. ISSN: 2666-7762 (May 2023).
 40. Susswein, Z. *et al.* Ignoring spatial heterogeneity in drivers of SARS-CoV-2 transmission in the US will impede sustained elimination. *medRxiv*. eprint: <https://www.medrxiv.org/content/early/2021/08/10/2021.08.09.21261807.full.pdf> (2021).
 41. Mazzoli, M., Valdano, E. & Colizza, V. Projecting the COVID-19 epidemic risk in France for the summer 2021. *Journal of Travel Medicine* **28**. ISSN: 1708-8305 (Oct. 2021).
 42. Jourdain, F. *et al.* From importation to autochthonous transmission: Drivers of chikungunya and dengue emergence in a temperate area. en. *PLOS Neglected Tropical Diseases* **14**. Publisher: Public Library of Science, e0008320. ISSN: 1935-2735 (2020).

-
43. Diekmann, O., Heesterbeek, J. A. P. & Metz, J. A. J. On the definition and the computation of the basic reproduction ratio R_0 in models for infectious diseases in heterogeneous populations. en. *Journal of Mathematical Biology* **28**, 365–382. ISSN: 1432-1416 (June 1990).
 44. Horn, R. A. & Johnson, C. R. *Matrix Analysis* ISBN: 0-521-38632-2 (Cambridge University Press, 1990).
 45. Iyer, S. *et al.* Large-scale measurement of aggregate human colocation patterns for epidemiological modeling. *Epidemics* **42**, 100663. ISSN: 1755-4365 (2023).
 46. White, L. F., Archer, B. & Pagano, M. Estimating the reproductive number in the presence of spatial heterogeneity of transmission patterns. *International Journal of Health Geographics* **12**, 35. ISSN: 1476-072X (July 2013).
 47. Trevisin, C. *et al.* Spatially explicit effective reproduction numbers from incidence and mobility data. *Proceedings of the National Academy of Sciences* **120**. Publisher: Proceedings of the National Academy of Sciences, e2219816120 (May 2023).
 48. Egleston, P. D., Lenker, T. D. & Narayan, S. K. The nonnegative inverse eigenvalue problem. en. *Linear Algebra and its Applications. Special Issue on the Tenth ILAS Conference (Auburn, 2002)* **379**, 475–490. ISSN: 0024-3795 (Mar. 2004).
 49. Kellogg, R. B. & Stephens, A. B. Complex eigenvalues of a non-negative matrix with a specified graph. en. *Linear Algebra and its Applications* **20**, 179–187. ISSN: 0024-3795 (Jan. 1978).
 50. Torre-Mayo, J., Abril-Raymundo, M. R., Alarcia-Estévez, E., Marijuán, C. & Pisonero, M. The nonnegative inverse eigenvalue problem from the coefficients of the characteristic polynomial. EBL digraphs. en. *Linear Algebra and its Applications* **426**, 729–773. ISSN: 0024-3795 (Oct. 2007).
 51. Schneider, C. M., Belik, V., Couronné, T., Smoreda, Z. & González, M. C. Unraveling daily human mobility motifs. *Journal of the Royal Society Interface* **10**. ISSN: 17425662 (2013).
 52. France, S. P. *COVID-19 : point épidémiologique du 11 février 2021* fr.
 53. Di Domenico, L., Sabbatini, C. E., Pullano, G., Lévy-Bruhl, D. & Colizza, V. Impact of January 2021 curfew measures on SARS-CoV-2 B.1.1.7 circulation in France. en. *Eurosurveillance* **26**. Publisher: European Centre for Disease Prevention and Control, 2100272. ISSN: 1560-7917 (Apr. 2021).

-
54. Colizza, V. & Vespignani, A. Epidemic modeling in metapopulation systems with heterogeneous coupling pattern: Theory and simulations. *Journal of Theoretical Biology* **251**, 450–467. ISSN: 0022-5193 (2008).
 55. Balcan, D. *et al.* Multiscale mobility networks and the spatial spreading of infectious diseases. *Proceedings of the National Academy of Sciences* **106**. Publisher: Proceedings of the National Academy of Sciences, 21484–21489 (Dec. 2009).
 56. Faucher, B. *et al.* Agent-based modelling of reactive vaccination of workplaces and schools against COVID-19. *Nature Communications* **13**, 1414 (Mar. 2022).
 57. Diekmann, O., Heesterbeek, J. & Roberts, M. The construction of next-generation matrices for compartmental epidemic models. *Journal of the Royal Society, Interface / the Royal Society* **7**, 873–85 (Nov. 2009).

Supplementary information

Supplementary Methods, Supplementary Figure 1 and Supplementary References 1-3.

Supplementary Information for

Estimates of the reproduction ratio from epidemic surveillance may be biased in spatially structured populations

Piero Birello^{1,+}, Michele Re Fiorentin², Boxuan Wang¹,
Vittoria Colizza¹, and Eugenio Valdano^{1,*}.

¹*Sorbonne Université, INSERM, Institut Pierre Louis d'Epidémiologie et de Santé Publique, F75012, Paris, France.*

²*Department of Applied Science And Technology (DISAT), Politecnico di Torino, C.so Duca degli Abruzzi 24, 10129, Torino, Italy.*

⁺ *Department of Mathematical Sciences “Giuseppe Luigi Lagrange” (DISMA), Politecnico di Torino, C.so Duca degli Abruzzi 24, 10129, Torino, Italy.*

^{*} *Corresponding author eugenio.valdano@inserm.fr*

Contents

1	Supplementary Methods	2
1.1	Estimate of incidence from hospital admissions data	2
1.2	Correction to within-community Colocation Maps	2
1.3	On the applicability of the Perron-Frobenius theorem	2
1.4	Generation interval and EpiEstim settings	3
2	Supplementary Figure	5
	Supplementary References	6

1 Supplementary Methods

1.1 Estimate of incidence from hospital admissions data

We estimate the incidence of COVID-19 infections (number of new infections per time interval per unit of population) in France from hospital admission data [1, 2]. Analogously to what we did in Ref. [2], we reconstruct incident infections $I(t)$ from incident hospitalizations $H(t)$ as follows: $I(t) = H(t + 7)/0.032$, where 0.032 is the average fraction of hospitalisations per infectious case and 7 is the average time from infection to hospitalization [3]. Hospitalization data come from the French Public Health Authority (*Santé Publique France*) and are accessible at <https://www.data.gouv.fr>.

1.2 Correction to within-community Colocation Maps

In the case of densely populated spatial patches, home-staying co-locations are likely to consistently increase the within-community mixing measured by Meta Colocation Maps [4]. Analogously to what we did in Ref. [2], we hence correct diagonal \mathbf{p} entries using Meta Movement Range Maps (see Data availability). Movement Range Maps give the average fraction sp_i of residents of community i that do not leave a given $600m \times 600m$ tile for the whole day. To be precise, data points include observations from 8 pm to 7:59 pm of the next day in local time. The probability $p_{ii}^{(sp)}$ to observe home-staying co-locations in community i is given by the ratio between the number of observed co-locations in that community, and all possible co-locations in it. In turn, the number of observed co-locations in i is given by the couples of people remaining home in each tile times the number of tiles in that patch. Then:

$$p_{ii}^{(sp)} = \frac{(sp_i d_i A)(sp_i d_i A - 1)m_i}{n_i(n_i - 1)}, \quad (1)$$

where d_i is the population density in community i , $A = 0.36 \text{ km}^2$ is the area of a single tile, m_i is the number of tiles occupied by community i and n_i is i 's population. We subtract $p_{ii}^{(sp)}$ to p_{ii} for each i .

1.3 On the applicability of the Perron-Frobenius theorem

The Perron-Frobenius theorem as used in the main paper requires that the matrix be strictly positive ($R_{ij} > 0$), or nonnegative ($R_{ij} \geq 0$) and irreducible. In our case \mathbf{R} may not be strictly positive if, for some i, j , cases from i generate no cases in j , so we shall prove here that it is irreducible, or that it can be made irreducible. A nonnegative

matrix is irreducible if and only if its associated directed graph is strongly connected [5]. The associated graph of \mathbf{R} is that which has a link between nodes i, j if $R_{ij} > 0$. In general, a suitable permutation of the node indices will bring \mathbf{R} to the following form, which mirrors the general bow-tie structure of the associated directed graph:

$$\mathbf{R} = \left(\begin{array}{c|c|c} \mathbf{T}_u & 0 & 0 \\ \hline \mathbf{B}_1 & \mathbf{R}_{scc} & 0 \\ \hline \mathbf{B}_2 & \mathbf{B}_3 & \mathbf{T}_d \end{array} \right). \quad (2)$$

where the blocks $\mathbf{T}_u, \mathbf{T}_d$ are lower diagonal and \mathbf{R}_{scc} is the adjacency submatrix of strongly connected component. The spectrum of \mathbf{R} is then the union of the diagonal elements of $\mathbf{T}_u, \mathbf{T}_d$ and the spectrum of \mathbf{R}_{scc} . Now three options are possible. First, if R , the spectral radius of \mathbf{R} and true reproduction ratio, is among the diagonal elements of \mathbf{T}_d this means that there is one community that sustains the epidemic and at most exports cases to other sink communities (remember \mathbf{T}_d is lower diagonal), so it is a trivial case with no actual epidemic dynamics between communities.

Second, if R belongs to the spectrum of \mathbf{R}_{scc} , then we shall write the Perron eigenvector in blocks as follows:

$$\mathbf{v} = \left(\begin{array}{c} \mathbf{v}_u \\ \hline \mathbf{v}_{scc} \\ \hline \mathbf{v}_d \end{array} \right). \quad (3)$$

If we write by blocks the eigenvector equation $\mathbf{R}\mathbf{v} = R\mathbf{v}$, on the top block we have $\mathbf{T}_u\mathbf{v}_u = R\mathbf{v}_u$, whose only solution is $\mathbf{v}_u = 0$ as R is not an eigenvalue of \mathbf{T}_u . This means $\mathbf{R}_{scc}\mathbf{v}_{scc} = R\mathbf{v}_{scc}$, and $\mathbf{v}_d = (R - \mathbf{T}_d)^{-1} \mathbf{B}_3\mathbf{v}_{scc}$, this being nonsingular because R is not an eigenvalue of \mathbf{T}_d . The dynamics is thus completely determined by the strongly connected component, and we can restrict our study to \mathbf{R}_{scc} , which represents by definition a strongly-connected graph and as such is irreducible, proving our initial claim.

Finally, if R is among the diagonal elements of \mathbf{T}_u again this means that there is one community that generates cases and exports them, possibly through several steps, to the strongly-connected component. Again this seeding part is trivial and underlies no actual epidemic dynamics between communities, so that again we can restrict our study to \mathbf{R}_{scc} .

1.4 Generation interval and EpiEstim settings

The generation interval is the time between infection and subsequent transmission to another individual. Estimating R through the R-package EpiEstim requires feeding the generation interval distribution associated to the disease[4]. We obtain here the generation

interval for our epidemic model.

The compartmental model we use (see Methods and Ref. [6]) has a rate of transition from the E to the I compartment (ϵ) and a recovery rate μ . We also define an effective transmissibility μR (see Eq. (15) of main paper). Let τ be the generation time. Let the probability that a transmission event occurs exactly after τ has passed since primary infection be $P(t)dt$. Also, let τ_E be the time one stays in the E compartment: $\tau_E \sim \text{Exp}(\epsilon)$, and τ_I be the time one stays in the I compartment: $\tau_I \sim \text{Exp}(\mu)$. Conditioning on τ_E, τ_I , we have

$$P(\tau|\tau_E, \tau_I)dt = \mu R dt \theta(\tau - \tau_E) \theta(\tau_I + \tau_E - \tau), \quad (4)$$

where θ is the Heaviside's function. So now we marginalize and get the generation time distributio $P(\tau)$:

$$P(\tau) = \int_0^\infty d\tau_E d\tau_I P(\tau|\tau_E, \tau_I) P(\tau_E) P(\tau_I) = \frac{\mu \epsilon R}{\mu - \epsilon} (e^{-\epsilon \tau} - e^{-\mu \tau}). \quad (5)$$

Note that a discrete distribution is required by the EpiEstim package. We choose to compute it over 50 bins in the interval $[0, 49]$. The time window over which to estimate R is set to be a week. In all simulations, we assign the estimate for R returned for the week interval $[t, t + 6]$ to the day $t + 3$. Also, given the smaller precision of early estimates, as reported in the documentation [4], we arbitrarily choose not to plot EpiEstim points associated to the first two weeks from the start of the synthetic epidemic.

2 Supplementary Figure

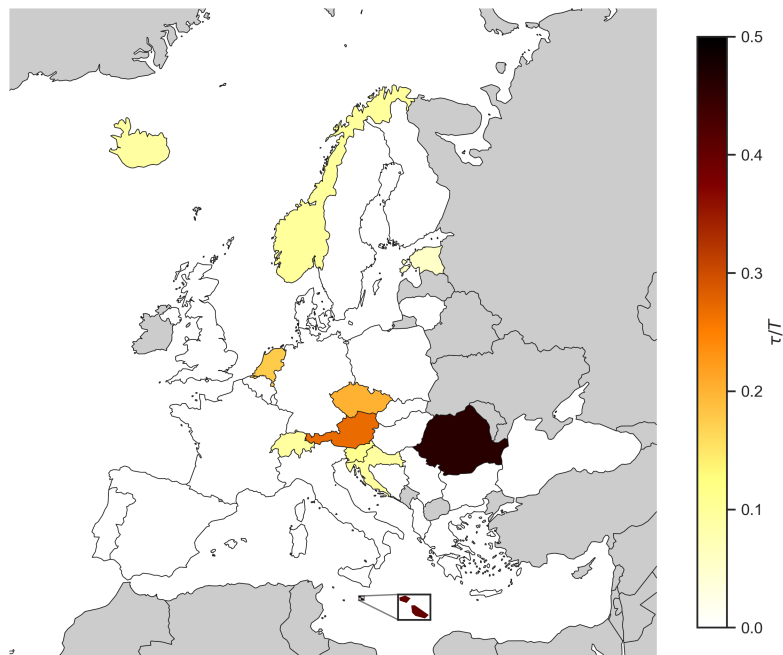


Fig.1|Decay time and oscillation period of the modes of $\Delta = S - R$ for selected European countries.

The color shows the value, for each country, $\max_{\alpha} \tau_{\alpha} / T_{\alpha}$, where $\tau_{\alpha}, T_{\alpha}$ are defined in the main paper and are, respectively, the decay time and the oscillation period of the α th mode. 32 countries are included: 24 members of the European Union (excluding Cyprus, Ireland and Latvia for lack of data) plus Albania, Bosnia and Herzegovina, Iceland, Montenegro, Norway, Serbia, Sweden, UK (see Data availability). Countries with real positive eigenvalues only are colored in white ($T_{\alpha} = \infty$), countries not included are in gray.

Supplementary References

1. Salje, H. *et al.* Estimating the burden of SARS-CoV-2 in France. *Science* **369**, 208–211. eprint: <https://www.science.org/doi/pdf/10.1126/science.abc3517> (2020).
2. Mazzoli, M., Valdano, E. & Colizza, V. Projecting the COVID-19 epidemic risk in France for the summer 2021. *Journal of Travel Medicine* **28**. ISSN: 1708-8305 (Oct. 2021).
3. Pullano, G. *et al.* Underdetection of COVID-19 cases in France threatens epidemic control. *Nature* **590** (Feb. 2021).
4. Cori, A., Ferguson, N. M., Fraser, C. & Cauchemez, S. A New Framework and Software to Estimate Time-Varying Reproduction Numbers During Epidemics. *American Journal of Epidemiology* **178**, 1505–1512. ISSN: 0002-9262 (Nov. 2013).
5. Horn, R. A. & Johnson, C. R. *Matrix Analysis* ISBN: 0-521-38632-2 (Cambridge University Press, 1990).
6. Faucher, B. *et al.* Agent-based modelling of reactive vaccination of workplaces and schools against COVID-19. *Nature Communications* **13**, 1414 (Mar. 2022).